ICAS 2021 SHANGHAI
International Council of the Aeronautical Sciences
32nd Congress of the International Council of the Aeronautical Sciences
September 6-10, 2021
Pudong Shangri-La, Shanghai, China

MODELING AND CONTROL OF A HOVERABLE FLAPPING WING AIRCRAFT CONSIDERING FLAPPING WING INDUCED FLOW

Liang Wang[1,2], Longfei Zhao[2,3,4], Wuyao Jiang[1,2], Zongxia Jiao[1,2,3]

[1]School of Automation Science and Electrical Engineering, Beihang University, Beijing 100191, China
[2]Science and Technology on Aircraft Control Laboratory, Beihang University, Beijing 100191, China
[3]Ningbo Institute of Technology, Beihang University, Ningbo 315800, China
[4]Research Institute for Frontier Science, Beihang University, 100191, Beijing, China

Abstract

Hovering modeling and control of Beihawk are presented in this paper. Beihawk, a 1.2 kg X-shaped flapping wing aircraft, is capable of vertical takeoff and landing. Unsteady effects including partial leading edge suction, flapping wing induced flow and post-stall behaviour were considered in wing aerodynamics modeling. Flapping-wing induced flow was crucial to tail control force generation in hover and low speed flight. Therefore, a periodically time-varying model considering this induced flow was established and furtherly simplified for control study. A proportional-derivative (PD) double loop controller was finally designed to cope with the underactuated and frequent attitude change characteristics of Beihawk. Simulation results indicated that the proposed controller could maintain the aircraft in stable hover.

Keywords: Flapping flight, unsteady effects, induced flow, periodically time-varying model, hover control

1. Introduction

Flapping flight can generate lift and thrust force simultaneously just relying on the beating of wings. It features with the merits of high flight efficiency, good maneuverability and compact structure. Presently, hoverable flapping-wing aircrafts are mostly small scaled, such as Nano Hummingbird [1], Delfly [2], Harvard Robobee [3], and so on. It is challenging to enable a large flapping-wing aircraft to hover stably due to their large flapping inertial force, such as Flapper [4], Slowhawk [5], Pterosaur Replica [6], and so on. In particular, this paper challenged the hovering modeling and control of a large flapping wing aircraft, Beihawk. It can perform hover and other high maneuvers by utilizing clap-fling mechanism (X-shaped wings design).

Great achievements have been made in modeling and control of flapping flight in the past few years. Aerodynamics of flapping-wing aircrafts are significantly different from that of conventional aircrafts due to their low-Reynolds number and unsteady viscous flow field. Existing aerodynamic models of flapping flight can be roughly divided into three catogories: steady models, quasi-steady models and unsteady models [7]. Traditional aerodynamic theory is adopted in steady models and the calculated aerodynamic forces remain constant at every moment. Quasi-steady models estimate the instantaneous forces based on instantaneous flapping velocity, while ignoring the flow field and time. Unsteady models provide more details of the flow field by including the unsteady phenomena related to vortices.

Presently, quasi-steady models are widely used in flapping flight controller design since it can predict the time history of wing forces for any kinematic pattern with low demands on computation power. Dickinson [8] derived an analytical quasi-steady model with force coefficients identified by experiment. This model was widely used in flapping flight control by Deng [9], Rifai [10] and good control effect has been made. X-shaped flapping wings can generate a steady momentum jet by oscillating back and forth. Hoff [11] firstly pointed out the similarity between this character of flapping wings and a propeller, and momentum theory was used to calculate the induced flow. However, momentum theory assumed this time-varying flow to be constant and the derived force was constant as well. To solve this problem, blade element theory including induced flow velocity, which has been widely used in the study of propellers, was applied to flapping flight by Harmon [12] and verified by experiment, approximately varying by 10% from the actual distribution. This variation is due to steady-state assumption, since quasi-steady assumption is valid for low value of reduced frequency, such as fast forward flight [13]. While during hovering stage, the flight velocity is zero and the reduced frequency becomes infinite [13].

Unsteady models can give a detailed description, based on finite element solution of Navier-Strokes equations. However, their implementation is unsuitable for control purposes since they require several hours of processing for simulating a single wing beat [14]. Recently, several advances have been achieved in comprehending qualitively and quantitatively unsteady effects, among which it was worth mentioning that Delaurier gave an analytical unsteady model [11]. Delaurier's model included low-fidelity representations of the 3-D unsteady effects, friction effects, a partial leading edge suction, and a post-stall behaviour. It has been used in the optimization of aerodynamic parameters by Zakaria et al [6].

Besides, the induced flow generated by the X-shaped wings is also a main source of Beihawk's tail flow especially during hovering stage. However, most of the researchers[15] supposed that flow over the tail equals to the relative flow caused by the flight velocity of Beihawk. This assumption might be valid in fast forward flight when the velocity of Beihawk exceeded this induced flow, but failed in hover.

In this paper, an unsteady model has been established for Beihawk in hover by adapting Delaurier's model and also including the induced flow derived from momentum theory. This model not only includes unsteady effects such as partial leading edge suction and post-stall behaviour, but also fully considers flapping-wing induced flow over the tail. Based on this model, an approximation method is proposed for controller design, and a PD double loop controller is thus designed, which enables Beihawk to achieve stable hover.

This paper is organized as follows. Section 2 gives a brief overview of Beihawk. Section 3 describes model of Beihawk, including wing aerodynamics, tail aerodynamics and body dynamics. Section 4 describes controller design based on model proposed in Section 3. Section 5 presents control effects by simulation. Section 6 summarizes conclusions and proposes some directions for future work.

2. Beihawk Overview

Beihawk has 1.5 m wingspan and weighs 1.2 kg. If proven flapping wing vector control techniques [9] were still adopted to drive the wing root, high control power was required to conteract the large inertial force, and the duration of flight would be significantly reduced. To address this, a special control mode was designed for Beihawk. Beihawk has four control channels including throttle, rudder propeller, and two channels for elevon. Throttle is realized by adjusting motor rotating speed, by which flapping frequency is capable of varying between 0-10Hz. Elevons are realized by two tail control surfaces installed on clap-fling plane and thus soaked in the strong axial induced flow to strengthen the control effect. Same polarity movement of the two surfaces generates pitch torque and different polarity deflection generates roll torque. Due to the gap of induced flow near x axis, a control surface won't work in hover at the position of a traditional vertical tail. Therefore, a two-way controllable tail propeller set was installed to actively generate yaw torque, similar to a normal helicopter tail rotor. Figure 1 shows a conceptual view of Beihawk. This paper mainly demonstrates Beihawk in hover, and thus

related control inputs are flapping frequency and same polarity movement of the two tail control surfaces.

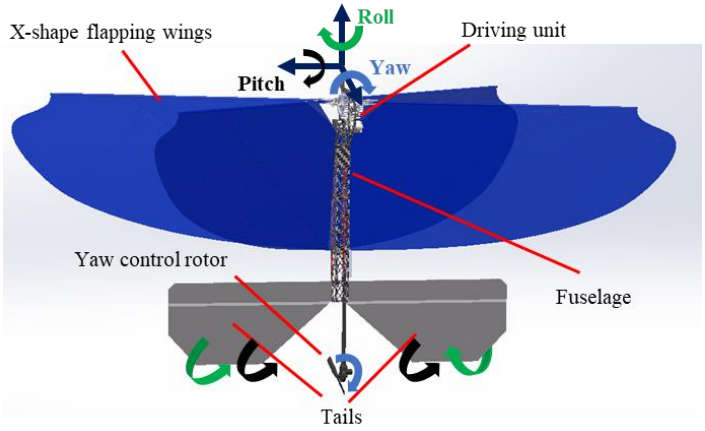

Figure 1 – Conceptual view of Beihawk

3. Beihawk Model

Figure 2 presents that a strong induced flow is generated between the wings and spreads along body axis. This flow is the main source of wing's incoming flow in hover and the tail is also soaked in this flow, specifying the induced flow is non-negligible in the aerodynamic modeling of Beihawk.

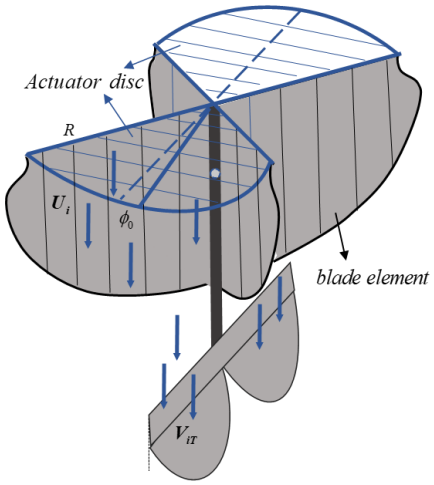

Figure 2 – Schematic diagram of model of Beihawk

3.1. Wing Aerodynamics

Delaurier's model [16] devides wing surface into blades along spanwise as shown in Figure 2 and assumes each blade has three distinct motions: forward motion, flapping motion and twisting motion. However, Delaurier's model requires incoming flow, which constrains its application in hover. Because the velocity of aircraft along the body axis is zero in hover. In this paper, momentum theory [17] is introduced to calculate induced flow velocity U_i as shown in Eq. (1) and this flow is used as the incoming flow in hover as shown in Figure 2.

$$U_i = \sqrt{\frac{W}{S_d}\frac{1}{2\rho}} \tag{1}$$

W is the weight, ρ is air density, and S_d is actuator disc area as shown in Figure 3.

Flapping and twisting motion of Beihawk are designed based on previous study by Jiao [18], assuming sine flapping angle and twisting angle within a flap cycle, arctangent twisting angle distribution along spanwise. The phase lag is set to be 90 deg, which has been proved to be efficient by Harijono [19]. The flapping angle ϕ and twisting angle β are thus given by

$$\begin{cases} \phi(t) = -\phi_{\max}\cos(2\pi ft) \\ \beta(t) = -\arctan(\dfrac{n}{N}\tan(\beta_{\max}))\sin(2\pi ft) \end{cases} (n = 1,...,N), \tag{2}$$

where $\phi_{\max}$ is the flapping amplitude, *f* is the flapping frequency, $\beta_{\max}$ is the twisting angle of the blade on the wing tip and it is also the maximum twisting angle, and *N* is the number of the wing blades of the wing.

The pitch angle of the airfoil chord with respect to the induced flow is given by

$$\theta_w = \beta(t) \tag{3}$$

Choose a random blade as an example to calculate the aerodynamic forces by adopting Delaurier's model and others are the same.

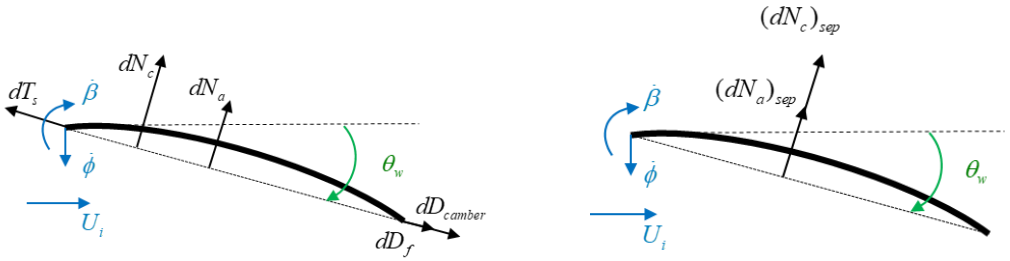

(a) Attached flow (b) Seperated flow

Figure 3 – Blade element aerodynamic forces

Normal force for attached flow can be written as

$$dN_c = \frac{1}{2}\rho U_i V C_n(x) c dy, \tag{4}$$

$$dN_a = \frac{\rho\pi c^2}{4}\dot{v}_2 dy, \tag{5}$$

$$dN = dN_a + dN_c, \tag{6}$$

where dN_c, dN_a, dN seperatedly represent circulatory normal force, added mass force, and total attached normal force.

Forces in the chordwise direction for attached flow are given by

$$dD_{camber} = -2\pi\alpha_0(\alpha' + \bar{\theta}_w)\frac{\rho U_i V}{2} c dy, \tag{7}$$

$$dT_s = \eta_s 2\pi(\alpha' + \bar{\theta}_w - \frac{1}{4}\frac{c\dot{\theta}_w}{U_i})\frac{\rho U_i V}{2} c dy, \tag{8}$$

$$dD_f = (C_d)_f \frac{\rho V_x^2}{2} c dy, \tag{9}$$

$$dF_x = dT_s - dD_{camber} - dD_f, \tag{10}$$

where dD_{camber}, dT_s, dD_f, dF_x seperately represent force due to camber, leading edge suction, friction drag, and total chordwise force.

When the flow is seperated, normal forces under seperated condition are expressed as

$$(dN_c)_{sep} = (C_d)_{cf} \frac{\rho \hat{V} V_n}{2} c dx , \tag{11}$$

$$(dN_a)_{sep} = \frac{1}{2}(dN_a) , \tag{12}$$

$$(dN)_{sep} = (dN_c)_{sep} + (dN_a)_{sep} , \tag{13}$$

where $(dN_c)_{sep}$, $(dN_a)_{sep}$, $(dN)_{sep}$ seperately represent force due to cross-flow drag, seperated apparent mass effects, and total seperated normal force.

When the flow is seperated, all chordwise forces are negligible. Definition of above parameters are the same as Delaurier [16].

Based on the above results, equations for the blade's instantaneous lift and thrust forces are

$$\begin{aligned} dL &= dN \cos\theta_w + dF_x \sin\theta_w \\ dT &= dF_x \cos\theta_w - dN \sin\theta_w \end{aligned} . \tag{14}$$

The motion of the up-wing and the down-wing are different due to the design of dihedral angle, i.e., ϕ_0 shown in Figure 2. Therefore, flapping motion and pitching motion of the up-wing and the down-wing can be seperatedly presented as follows,

$$\begin{aligned} \phi_{up}(t) &= \phi_{\max} \cos(2\pi ft) - \phi_0 \\ \phi_{down}(t) &= -\phi_{\max} \cos(2\pi ft) - \phi_0 \\ \beta_{up}(t) &= \arctan(\frac{n}{N} \tan(\beta_{\max})) \sin(2\pi ft) \\ \beta_{down}(t) &= -\arctan(\frac{n}{N} \tan(\beta_{\max})) \sin(2\pi ft) \end{aligned} . \tag{15}$$

The whole wings' instantaneous lift and thrust forces are given by integration

$$\begin{aligned} L(t) &= 2\left[\int_0^{b/2} \cos\phi_{up} dL_{up} + \cos\phi_{down} dL_{down}\right] \\ T(t) &= 2\left[\int_0^{b/2} dT_{up} + dT_{down}\right] \end{aligned} \tag{16}$$

Kinematic and aerodynamic parameters of Beihawk are seperately listed in Table 1 and Table 2. The wing of Beihawk is divided into 12 blades of equal width (dy = 0.0625 m) as listed in Table 3. The calculated lift force and thrust force of one wing during a flapping period with 8Hz flapping frequency are shown in Figure 4.

Table. 1 Kinematic parameters for Beihawk

Parameter	Value
m	0.8 kg
b	1.5 m
S_{Tail}	0.1 m^2
$\phi_{\max}$	15 deg
$\beta_{\max}$	50 deg

Table. 2 Aerodynamic parameters for airfoil

Parameter	Value
α_0	0.5 deg
η_s	0.98
$(\alpha_{stall})_{\max}$	13 deg
$(\alpha_{stall})_{\min}$	-13 deg

Table. 3 Mean chord of 12 blades for Beihawk

No	1	2	3	4	5	6	7	8	9	10	11	12
c/m	0.25	0.25	0.23	0.22	0.21	0.20	0.19	0.18	0.16	0.14	0.12	0.10

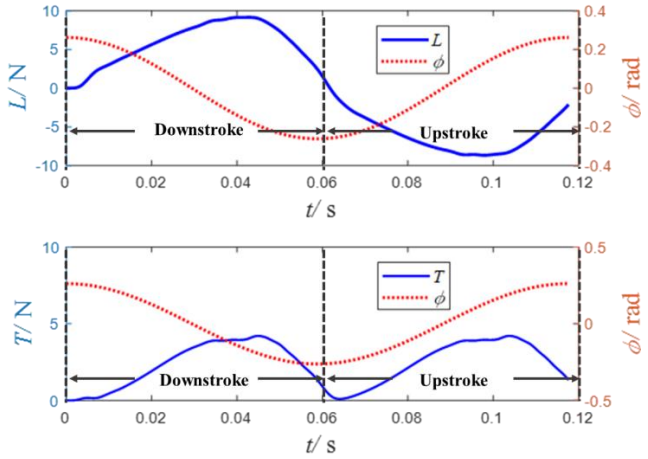

Figure 4 – Lift and thrust force of one wing during one flapping period with 8 Hz flapping frequency

Figure 4 presents that the corresponding lift force and thrust force are positive during downstroke, which is consistent with the actual positive attack angle. While during upstroke the corresponding lift force and thrust force are seperately negative and positive. This also coincides with the actual negative attack angle. Figure 4 also shows that the averaged lift force is nearly zero and the averaged thrust force of the four wings is almost 12 N under 8 Hz flapping frequency. This is also basically the same as the 8 Hz hovering frequency in experiment.

Due to the design of dihedral angle, the aerodynamic center of the wing, A_W, is located above the center of gravity, G, as shown in Figure 5. Pitch torque generated by the wings owing to the lift and thrust forces can be evaluated as follows,

$$M_W(t) = L(t) \bullet x_W^0 - T(t) \bullet z_W^0 \tag{17}$$

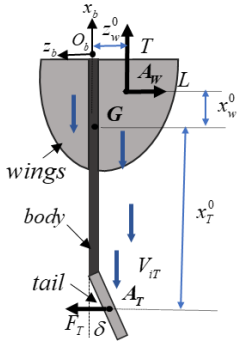

Figure 5 – Schematic diagram of Beihawk during hovering stage

3.2. Tail Aerodynamics

Flapping-wing induced flow is also the source of incoming flow over the tail. Therefore, momentum theory [12] is also used here to calculate the flow over the tail. $V_i(0)$ is the velocity of the induced flow at wing root and given by

$$V_i(0)=0.5\sqrt{\frac{T}{S_d}\frac{1}{2\rho}} \tag{18}$$

where *T* is the thrust force and is a function of *f*. Distribution of the induced flow, V_i, increases along the body and obeys the following rule,

$$V_i(x)=V_i(0)\left[1+\frac{x/R}{\sqrt{1+(x/R)^2}}\right] \tag{19}$$

where *R* is the diameter of the actuator disk, equalling to *b*/2 for Beihawk, and *x* position is the distance from the wing root along the body. Beihawk's tail is installed at approximately 0.5 *m* from the wing root and the induced flow velocity at the tail, i.e., V_{iT}, can be obtained.

The tail is installed as a panel. Thus, bernoulli's equation can be used to calculate the aerodynamic force acting on the tail,

$$F_T(t)=\frac{1}{2}\rho V_{iT}^2 S_{tail} C_{L-tail} \tag{20}$$

where S_{tail} is the area of the tail, and C_{L-tail} is the aerodynamic coefficient of the tail and equals to $2\pi\delta$ for relative small δ, i.e., the tail pitch angle. The aerodynamic center of the tail force, A_T, is shown in Figure. 5 and the corresponding torque is given by

$$M_T(t)=F_T(t)\bullet x_T^0 \tag{21}$$

where x_T^0 is the distance between A_T and *G* along *x* axis. Note that the torque of the tail, M_T, is determined by both tail pitch angle and flapping frequency, which is also the unique of our model.

3.3. Body Dynamics

Different from fixed-wing aircraft, flapping-wing aircraft is a typical multi-body system [20]. Although the inertia force of Beihawk is non-negligible, X-shaped wing design makes the inertial forces in the opposite moving direction cancel out. The internal forces between the rigid bodies will not have significant influence on the motion of the whole system. Therefore, it is reasonable to adopt single-body model and the longitudinal dynamics in inertial frame are given by

$$\begin{aligned}
&\dot{x}^*(t)=u^*(t)\\
&\dot{u}^*(t)=\frac{1}{m}\left[T(t)\cos\theta^*(t)-(L(t)-F_T(t))\sin\theta^*(t)\right]-g\\
&\dot{z}^*(t)=w^*(t)\\
&\dot{w}^*(t)=\frac{1}{m}\left[-T(t)\sin\theta^*(t)-(L(t)-F_T(t))\cos\theta^*(t)\right]\\
&\dot{\theta}^*(t)=q^*(t)\\
&\dot{q}^*(t)=\frac{1}{I_{yy}}(M_W(t)+M_T(t))
\end{aligned}, \tag{22}$$

where $L(t)$, $T(t)$, $F_W(t)$, $M_W(t)$, $M_T(t)$ are all periodically time-varying forces due to the periodic flapping motion. This is also the most important feature of flapping-wing aircrafts.

4. Flight control

4.1 Simplified model

Model proposed in Section 3 is a nonlinear periodically time-varying system. It is complicated to design a controller for such a non-autonomous system since its response relies on initial time apart from control inputs. Considering the fact that the flapping frequency is much larger than the body natural frequency, averaging theory is applied to transform such a non-autonomous system into an autonomous system, i.e., a time-averaged model. The wing's averaged lift and thrust forces are obtained by integrating $L(t)$ and $T(t)$ over the cycle after substituting $\Gamma=2\pi ft$,

$$\begin{aligned}\bar{L} &= \frac{1}{2\pi}\int_0^{2\pi} L(\Gamma)d\Gamma \\ \bar{T} &= \frac{1}{2\pi}\int_0^{2\pi} T(\Gamma)d\Gamma\end{aligned} \tag{23}$$

The mean lift force and mean torques generated by the wing equal to zero within a flapping period in hover. The mean thrust force can balance the weight. Therefore, model applied for controller design can be a simplification of Eq. (22) and is given by

$$\begin{aligned}\dot{x} &= u \\ \dot{u} &= \frac{1}{m}\bar{T}\cos\theta - g \\ \dot{z} &= w \\ \dot{w} &= -\frac{1}{m}\bar{T}\sin\theta \\ \dot{\theta} &= q \\ \dot{q} &= \frac{1}{I_{yy}}\bar{M}_T\end{aligned} \quad . \tag{24}$$

$\bar{T}$ and $\bar{M}_T$, cannot be directly used to control Beihawk since the control input are frequency and tail pitch angle. The aerodynamic model proposed in section 3 is used to calculate the corresponding f and δ based on $\bar{T}$ and $\bar{M}_T$. However, the nonlinear map between them cannot be computed analytically, since the aerodynamic forces and torques are complex functions of frequency and tail pitch angle. Therefore, an approximation method is proposed to solve for the inverse transformation. Models presented in section 3 are integrated together to give a realistic simulation for Beihawk. Corresponding averaged thrust force can be obtained by changing the frequency. 100 sets of data are obtained by the variation of frequency between 0Hz to 10Hz at a step size of 0.1Hz and the results are shown in Figure. 6.

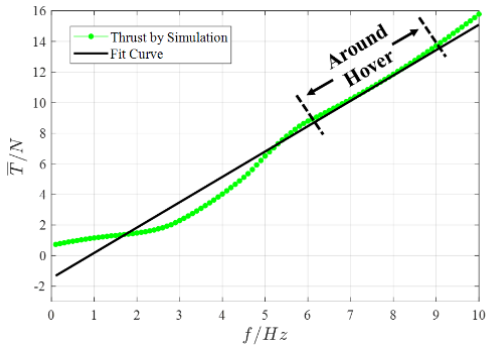

Figure 6 – Frequency and corresponding thrust force fitting results

It can be seen from Figure 6 that a linear correlation exists between the thrust and frequency around 8Hz, the hovering flapping frequency of Beihawk. By doing numerical fitting, relationship between them is given by

$$\bar{T} = 1.608 f - 4.336 \tag{25}$$

This result is also used to derive the tail torque. Based on the tail model in section 3.2 and Eq. (25), $\bar{M}_T$ is given by

$$\bar{M}_T = 0.3(1.608 f - 4.336)\delta \tag{26}$$

Eq. (25) and (26) are approximation of the wing and tail aerodynamics in hover, based on which, the inverse transformation of the aerodynamic model can be obtained. That is to say, corresponding frequency and tail pitch angle can be obtained according to the expected force and torque. A great deal can be made between accuracy and complexity by using the above method.

4.2. Controller design

Typically, the aircraft needs to adjust its position and attitude several times during flight. Therefore, PD double loop control is adapted for hovering control of Beihawk and the control structure is shown in Figure 7.

The inner loop is designed to be attitude control and the outer loop is designed to be position control. Given the expected vertical position x_d and horizontal position z_d, and the corresponding feedback values *x* and *z*, the outer loop controllers can output the expected vertical and horizontal acceleration. Thus, the expected thrust force, $\bar{T}_d$, and expected pitch angle, θ_d, can be obtained. The expected torque can be obtained by the inner loop controller based on θ_d and the corresponding feedback value θ. The expected torque and force are input into the inverse of the approximated aerodynamic models shown in Eq. (25) and (26), and the corresponding control input *f* and δ are thus obtained. Finally, *f* and δ are used to control Beihawk. The specific calculation process will be presented as follows.

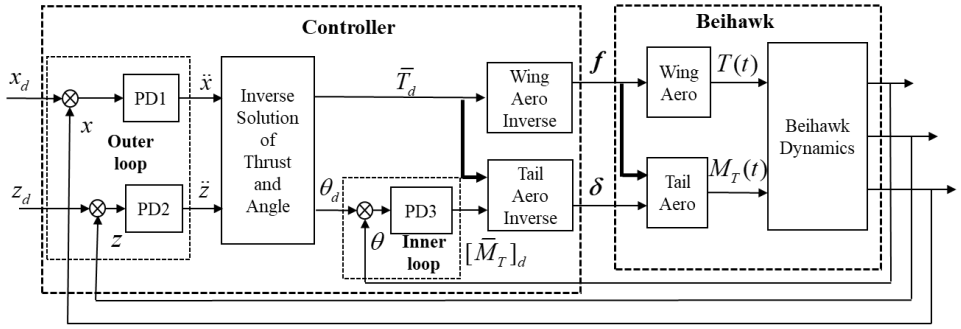

Figure 7 – Control structure of Beihawk

The position controllers, PD1 and PD2, output two virtual control variables: U_y and U_z, which are thought to be the corresponding accelerations.

$$\begin{aligned}\ddot{x} &= U_y = K_{p1}(x - x_d) + K_{d1}(\dot{x} - \dot{x}_d) \\ \ddot{z} &= U_z = K_{p2}(z - z_d) + K_{d2}(\dot{z} - \dot{z}_d)\end{aligned} \tag{27}$$

These virtual control variables are substituded into Eq. (24), and the expected thrust force and pitch angle can be given by

$$\bar{T}_d = m\sqrt{(U_x + g)^2 + U_z^2} \tag{28}$$

$$\theta_d = \arcsin\left[-\frac{U_z}{\sqrt{(U_x + g)^2 + U_z^2}}\right] \tag{29}$$

The attitude controller PD3 also outputs a virtual control variable, U_θ. The virtual control variable is thought to be the corresponding torque.

$$\left[\bar{M}_T\right]_d = U_\theta = K_{p3}(\theta - \theta_d) + K_{d3}(\dot{\theta} - \dot{\theta}_d) \tag{30}$$

Frequency *f* is obtained based on $\bar{T}_d$ by solving the inverse of the wing aerodynamics, i.e., Eq. (25). Tail pitch angle is obtained based on both $\bar{T}_d$ and $[\bar{M}_T]_d$ by solving the inverse of the tail aerodynamics, i.e., Eq. (26). This is also the advantage of our controller: flapping-wing induced flow is considered when designing tail controller.

θ_d is generated by outer loop control, which serves as the command of the inner loop. θ tracks θ_d through the inner loop control and the tracking error would influence the stability of the whole system. Therefore, the control gain of the inner loop is designed to be larger than the outer loop. Parameters of the controller are designed according to the pole assignment and listed in Table. 4..

Table. 4 Parameters for the controllers

Parameter	P1	D1	P2	D2	P3	D3
Value	9	6	9	6	25	10

5. Flight Control Results

The effectiveness of the controller designed in section 4 is demonstrated by simulations in the pitch-plane and the results are presented below.

Figure 8 (a)-(c) presents the tracking ability of the designed controller and the aircraft converges to hover status at the ideal position within 5 seconds. Small ripple exists in the vertical tracking, which results from the fact that the thrust force is time varying due to the periodic flapping motion of the wings. Figure 8 (d) shows that flapping frequency is held constant over a period of wing flap in order to avoid changing the sine shape of the flapping waveform. While tail pitch angle is adjusted over a period to cope with the disturbance of the time-varying induced flow velocity. In a word, controller designed based on cycle-averaged model can maintain the aircraft in hover with relatively small errors.

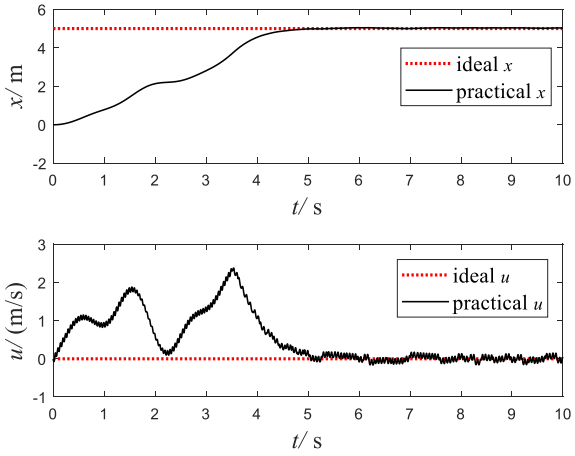

(a) Vertical tracking

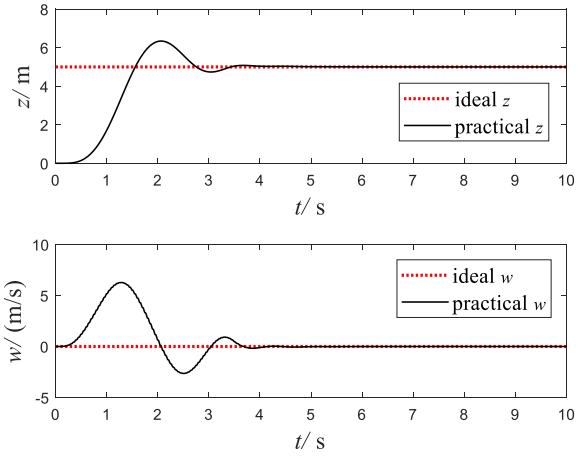

(b) Horizontal tracking

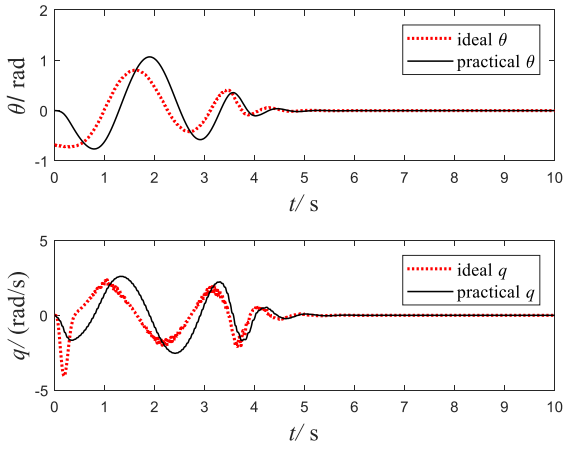

(c) Pitching angle tracking

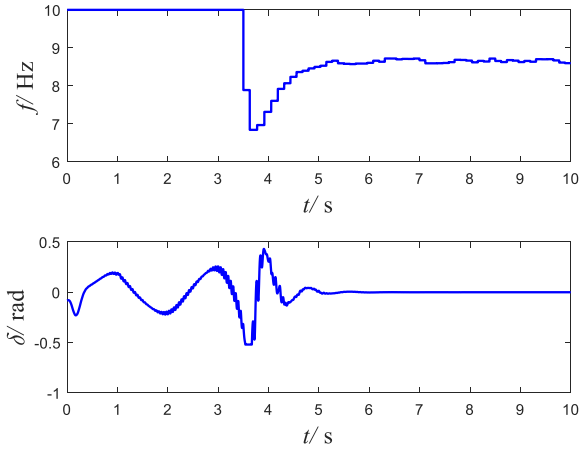

(d) Control inputs

Figure 8 – Tracking results under designed controller and corresponding control inputs

Traditional controller, PD controller without considering flapping-wing induced flow is compared with controller designed in this paper and the results are presented in Figure 9. It can be seen that the tracking ability of the traditional PD controller is not satisfying. Due to the lack of analysis of tail flow field, improper tail pitch angle response occurred in the control process. Attitude control will be overshoot and position control will also be influenced. Comparisons between these two controllers indicate the necessarity of considering flapping-wing induced flow in hovering control.

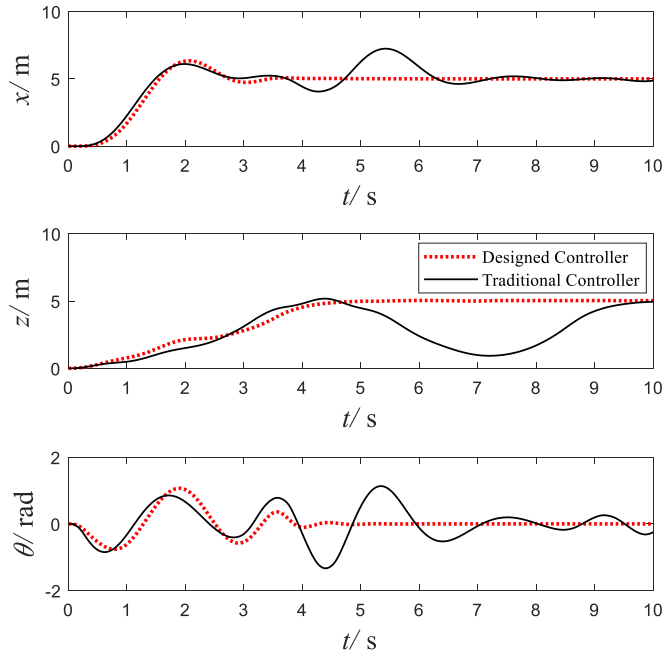

Figure 9 – Comparisons between traditional controller and designed controller

Controller's response to external torque disturbances is furtherly tested. A 0.5 N*m torque disturbance lasting for about a second is applied to the aircraft at 7 second and the response is shown in Figure 10. The aircraft can resist this torque disturbance by adjusting the tail pitch angle.

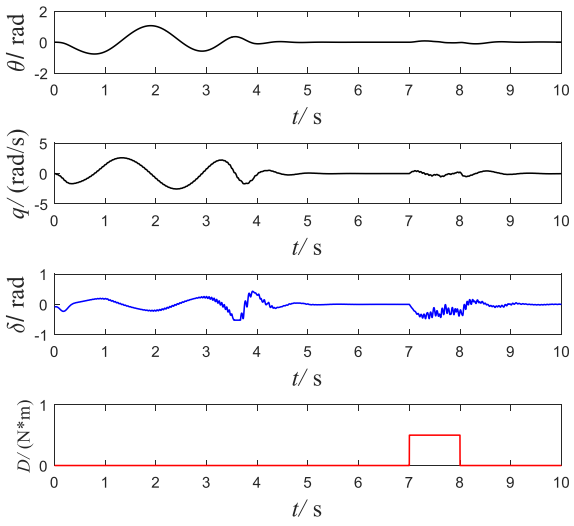

Figure 10 – Attitude tracking response to disturbance

6. Conclusion

In this paper, a large flapping-wing aircraft, Beihawk, equipped with stable hover capacity is introduced. The first major contribution of this paper is proposing a suitable unsteady model for controller design, which can give a detailed description of aerodynamics and be easily incorporated into dynamic model as well. The second major contribution is proposing a tail model considering flapping-wing induced flow and designing attitude controller based on this model. The controller can maintain Beihawk in stable hover within 5 seconds.

In this paper, only induced flow is considered and the relative flow aroused by the flight velocity is ignored. Induced flow over the tail tends to be disturbed by this verticle relative flow during fast vertical ascent or descent. Thus, tail control torque would be disturbed and pitching attitude of Beihawk may be out of control. This phenomenon is dangerous and should be avoided in actual flight. Furture research can pay attention to the stability region of Beihawk's attitude control under verticle relative flow disturbance.

7. Contact Author Email Address

Mailto: zhaolf@buaa.edu.cn

8. Copyright Statement

Reference

[1] Warrick DR, Tobalske BW, Powers DR. Aerodynamics of the hovering hummingbird. *Nature*, Vol. 435, No. 7045, pp 1094-1097, 2005.

[2] De Croon GCHE, Groen MA, De Wagter C, Remes B, Ruijsink R, Van Oudheusden BW. Design, aerodynamics and autonomy of the DelFly. *Bioinspiration and Biomimetics*, Vol. 7, No. 2, 2012.

[3] Robert Wood RN and G-YWS. Flight of the robobees. *Sci Am*, Vol. 308, No. 3, pp 60-65, 2013.

[4] Larijani RF, Delaurier JD. A nonlinear aeroelastic model for the study of flapping wing flight. *Fixed Flapping Wing Aerodyn Micro Air Veh Appl*, pp 399-428, 2001.

[5] Zakaria MY, Elshabka AM, Bayoumy AM, Elhamid OEA. Numerical aerodynamic characteristics of flapping wings. *13th International Conference on AEROSPACE SCIENCES & AVIATION TECHNOLOGY,* Cairo, Egypt, pp1-15, 2009.

[6] Zakaria MY, Taha HE, Hajj MR. Design optimization of flapping ornithopters: The pterosaur replica in forward flight. *J Aircr*, Vol. 53, No. 1, pp 48-59, 2016.

[7] Xuan H, Hu J, Yu Y, Zhang J. Recent progress in aerodynamic modeling methods for flapping flight. *AIP Adv*, Vol. 10, No. 020701, 2020.

[8] Sane SP, Dickinson MH. The aerodynamic effects of wing rotation and a revised quasi-steady model of flapping flight. *J Exp Biol*, Vol. 205, No. 8, pp 1087-1096, 2002.

[9] Deng X, Schenato L, Sastry SS. Flapping flight for biomimetic robotic insects: Part II - Flight control design. *IEEE Trans Robot*, Vol. 22, No. 4, pp 789-803, 2006.

[10] Rifaï H, Guerrero-Castellanos JF, Marchand N, Poulin G. Bounded attitude control of a flapping wing micro aerial vehicle using direct sensors measurements. *Proc - IEEE Int Conf Robot Autom*, pp 3644-3650, 2009.

[11] Hoff W. Der Flug der Insekten und der Vögel. *Naturwissenschaften*, Vol. 7, No. 10, pp 159-162, 1919.

[12] Harmon RL, Grauer J, Hubbard JE, et al. Experimental determination of ornithopter membrane wing shapes used for simple aerodynamic modeling. In: *26th- AIAA Applied Aerodynamics Conference AIAA Applied Aerodynamics Conference*, Honolulu, Hawaii, pp 1-17, 2008.

[13] Street D. The aerodynamics of hovering insect flight. *Phil Trans R Soc Lond*, Vol. 305, No. 2, pp 1-15, 1984.

[14] Deng X, Schenato L, Sastry SS. Flapping Flight for Biomimetic Robotic Insects: Part I—System Modeling. *IEEE Trans Robot*, Vol. 22, No. 4, pp 776-788, 2006.

[15] Rashid T. The flight dynamics of a full-scale ornithopter. 1995.

[16] DeLaurier JD. An aerodynamic model for flapping-wing flight. *Aeronaut J*, Vol. 97, No. 1853, pp 125-130, 1993.

[17] Robyn Lynn Harmon. Aerodynamic modelling of a flapping membrane wing using motion tracking experiments. 2008.

[18] Jiao Z, Zhao L, Shang Y, Sun X. Generic analytical thrust-force model for flapping wings. *AIAA J*, Vol. 56, No. 2, pp 581-593, 2018.

[19] Djojodihardjo H, Ramli ASS, Wiriadidjaja S. Kinematic and aerodynamic modelling of flapping wing ornithopter. *International Conference on Advances Science and Contemporary Engineering*. Vol 50, Jakarta, Indonesia, pp 848-863, 2012.

[20] Grauer JA, Hubbard JE. Multibody model of an ornithopter. *J Guid Control Dyn*, Vol. 32, No. 5, pp 1675-1679, 2009.